THE JOURNAL OF PHYSICAL CHEMISTRY A

ARTICLE

pubs.acs.org/JPCA

Adhesion through Single Peptide Aptamers

Marie-Eve Aubin-Tam,[†,‡] David C. Appleyard,[†,§] Enrico Ferrari,[∥,#] Valeria Garbin,[⊥] Oluwatimilehin O. Fadiran,[▽] Jacquelyn Kunkel,[‡] and Matthew J. Lang*[,‡,§,@]

[‡]Department of Mechanical Engineering and [§]Department of Biological Engineering, Massachusetts Institute of Technology, 77 Massachusetts Avenue, Cambridge, Massachusetts 02139, United States

[∥]Laboratorio Nazionale TASC Basovizza, CNR-INFM, 30142 Trieste, Italy

[⊥]Department of Chemical and Biomolecular Engineering, University of Pennsylvania, Philadelphia, Pennsylvania 19104, United States

[▽]Mechanical Engineering Department, University of Maryland Baltimore County, Baltimore, Maryland 21250, United States

ABSTRACT: Aptamer and antibody mediated adhesion is central to biological function and is valuable in the engineering of "lab on a chip" devices. Single molecule force spectroscopy using optical tweezers enables direct nonequilibrium measurement of these noncovalent interactions for three peptide aptamers selected for glass, polystyrene, and carbon nanotubes. A comprehensive examination of the strong attachment between antifluorescein 4−4−20 and fluorescein was also carried out using the same assay. Bond lifetime, barrier width, and free energy of activation are extracted from unbinding histogram data using three single molecule pulling models. The evaluated aptamers appear to adhere stronger than the fluorescein antibody under no- and low-load conditions, yet weaker than antibodies at loads above ∼25 pN. Comparison to force spectroscopy data of other biological linkages shows the diversity of load dependent binding and provides insight into linkages used in biological processes and those designed for engineered systems.

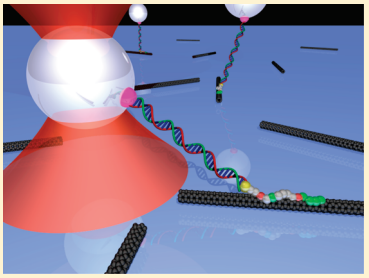

1. INTRODUCTION

Noncovalent interactions drive a myriad of biological processes such as association, adhesion, motility, structural rearrangement, and signaling. Aptamers[1] and antibodies are two broad categories of biomolecules with specific binding affinity, enabling applications in sensing,[2] diagnostic,[3] drug delivery,[4] imaging,[5] and therapy.[6,7] Peptide aptamers typically contain 8−20 amino acids and bind materials or biomolecules. They can be engineered via selection from large libraries of random sequences ($\sim 10^{10}$) by directed evolution techniques such as phage display. Antibodies are much larger and have hypervariable regions of over 60 residues susceptible to interact with an antigen, allowing high specificity and fine-tuned adhesion for reversibility.

Force-based studies of aptamer and antibody dissociation kinetics offer unique insight into the energetic landscape underlying these interactions as well as direct quantification of bond lifetimes under load. Despite the nonequilibrium nature of biological processes, bulk adhesion methods (surface plasmon resonance, ELISA, radioligand assay) are limited to measurements of unloaded bond lifetimes. Driving the system out of equilibrium is necessary for probing tight binders with extremely slow off-rates. Single molecule force spectroscopy is an invaluable tool to pry apart molecular interactions in nonequilibrium conditions; capable of quantifying bond strength and lifetimes by surveying the reaction coordinate,[8] in addition to exposing individual contributions underlying a population distribution. Further examination of unbinding forces of peptide aptamers and their loading rate dependence reveal the physical interactions governing adhesion, opening possibilities for engineering and modeling linkages for biologically guided assembly of materials.

Not only are aptamers important for guided and self-assembly of larger materials, but they are valuable in single molecule assay design. These complex assays are challenging to construct and rely upon the availability of various linkers and points of adhesion that must be both strong and specific allowing for the isolation of the desired molecular interaction. Aptamers offer a novel single molecule linkage that is specific, readily commercially available, very easy to engineer into a system, and small in size compared to linkers including streptavidin and antibodies. Comprehensively measuring the behavior under load for both aptamers and antibodies allows them to be correctly engineered into an assay and their contribution to the force response of the system to be accurately decoupled.

Although a majority of research has been focused on elucidation of aptamer sequences and applications, a minority has explored the mechanism of adhesion and an even smaller subset of these have extracted valuable force and kinetic parameters. A wide range of force measurements have been made using a naturally occurring aptamer, ferritin, obtaining adhesion strengths on Ti, Si, and Au ranging from 0.25 to 2 nN when probed with an atomic force microscope, AFM.[9] However,

Special Issue: Graham R. Fleming Festschrift

Received: April 7, 2010
Revised: August 11, 2010
Published: August 26, 2010

ferritin is a multi-subunit protein over 20 kDa in size, and the interactions could not be isolated to individual peptide sequences. Lee et al. designed a single molecule assay to probe an adhesive amino acid, dihydroxyphenylalanine, DOPA, a modification of tyrosine used by marine mussels.[10] DOPA adheres to both organic and inorganic surfaces, and the rupture distribution from a titanium surface was measured with a mean of 805 pN using an AFM. Binding by a 12 amino acid peptide designed by phage display for adhesion to chlorine-doped polypyrrole, PPyCl, was examined with an AFM by Sanghvi et al.[11] Unbinding force distributions with a mean of 112 pN were determined, yet, explicit control for single molecule rupture was not made. Although these studies highlight the importance of quantification of adhesive force, a broader understanding can be achieved through rigorous single molecule measurement. Here, optical tweezers are used to investigate peptide aptamers with high affinity for specific materials (carbon nanotubes,[12] polystyrene,[13] and glass[14]) and, for comparison, to probe a tightly binding antibody for fluorescein. Our aptamer measurements extend initial forays examining adhesion forces of biomolecules on surfaces by explicitly reaching the single molecule limit and obtaining rupture force histograms, thus providing extensive information relating to the rupture coordinate including bond lifetimes (τ(F)), barrier width ($x^{\ddagger}$), and free energy of activation ($\Delta G^{\ddagger}$). The bond lifetime under zero force (τ_0), $x^{\ddagger}$, and $\Delta G^{\ddagger}$ are found to be larger for peptide aptamers than for antifluorescein. Peptide aptamers are found to have longer lifetimes under low forces than antifluorescein; however, under forces higher than ~25pN, antifluorescein lifetime exceeds that of the aptamers.

2. EXPERIMENTAL SECTION

Single molecule studies are composed of a wet lab assay to isolate single tethers physically attached to the probe bead, an optical-trap-based force spectroscopy to measure the strength of the interaction, and data analysis to extract parameters relating to the underlying reaction coordinate. The general principals guiding assay design are based on foundational single molecule studies of motility[15] and structure.[16]

2.1. Single Molecule Pulling Assay. Figure 1 is a cartoon view of the geometry of a single molecule optical trap assay for aptamer adhesion to a carbon nanotube. A polystyrene bead (A) is used as a handle for the optical trap to apply force. The bead is attached to the aptamer (D) via a DNA linker (C) and biotin/streptavidin attachment chemistry (B). The glass, polystyrene, and antibody−antigen measurements follow a very similar assay geometry. Nonspecific interactions are mitigated by blocking available surfaces with casein. Long dsDNA linkers are used to minimize potential surface interactions from the microbead and to reduce the angle in the pulling geometry. For the peptide adhesion measurements, 3500 bp DNA tethers, 1.190 μm in length, are synthesized via PCR using a biotin conjugated forward primer (5′ - biotin - AAT CCG CTT TGC TTC TGA CT - 3′, IDT) and an amine conjugated reverse primer (5′ - amine - TTG AAA TAC CGA CCG TGT GA - 3′) on a M13mp18 plasmid (Bayou Biolabs). A cysteine and two glycine residues (CGG) are added at the N-terminus of the glass binding peptide (CGGRSGRRRSHHHRL), the polystyrene binding peptide (CGGRAFIASRRIKRP), and the carbon nanotube (CNT) binding peptide (CGGHWSAWWIRSNQS). DNA is conjugated to this N-terminal cysteine via the single amine group on DNA using sulfosuccinimidyl 4-[N-maleimidomethyl] cyclohexane-1-carboxylate (sulfo-SMCC, Pierce). For the anti-fluorescein adhesion measurements, 1100 bp DNA tethers, 0.374 μm in length, are obtained with a biotin conjugated forward primer (5′ - biotin - TAT TGC GTT TCC TCG GTT TC - 3′) and a fluorescein conjugated reverse primer (5′ - FI - TTG AAA TAC CGA CCG TGT GA - 3′). Assay conditions are optimized to ensure that beads are linked to the surface by a single tether.

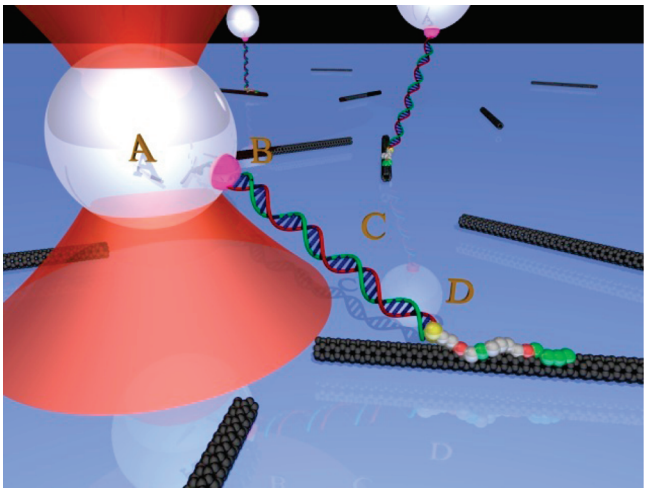

Figure 1. Schematics of optical tweezers pulling on a single peptide aptamer molecule linked to a carbon nanotube. The optical trap (red cone) captures a bead (A) that is linked to an aptamer (D) via a DNA molecule (C) and a biotin/streptavidin linkage (B).

A 15 μL flow chamber is prepared by attaching a KOH-etched coverslip to a microscope slide with double-sided tape. The sample is loaded on one side of the channel and buffer can be exchanged with the use of a pipet tip connected to a vacuum pump to provide suction at the other side.

In the glass binding assay, the DNA−peptide (DNA-CGGRSGRRRSHHHRL) conjugate is loaded in the channel at a concentration of 10 ng/uL in PBST (phosphate buffered saline, pH 7.4, with 0.01% Tween) and incubated 1 h at room temperature, RT. 1 mg/mL casein in PBST is then loaded into the channel and incubated for 30 min. At the same time, 0.80 μm polystyrene beads coated with streptavidin (Spherotech) are also incubated in 1 mg/mL casein in PBST for 30 min. Next, the beads are loaded in the channel, incubated for 30 min, and a final wash of the channel is made using 1 mg/mL casein solution. Tethered beads exhibit a tethered diffusion or "wobble".

In the polystyrene binding assay, in order to minimize non-specific binding, coverslips are coated with a layer of aminosilane, which are then reacted with a mixture of 99% NHS−PEG and 1% NHS−PEG−biotin (MW 5000, Laysan Bio.) for 4 h at RT. Chambers built with PEG-coated coverslips are incubated with 0.1 mg/mL streptavidin in PBST for 30 min and then with the 1.025 μm polystyrene beads (Polysciences). The beads are preincubated with 0.05 ng/μL of peptide−DNA conjugate (DNA-CGGRAFIASRRIKRP) for 3 h at 4 °C, spun down at 10000 rpm for 6 min, and resuspended in 1 mg/mL casein in PBST. This assay is inverted compared to that of the glass or carbon nanotubes, with the aptamer binding to the bead rather than the slide surface. A 30 min incubation at RT of the beads−peptide−DNA solution in the microscope slide chamber allows attachment of the DNA to the functionalized PEG surface. A final wash step using 100 μL of PBST removes unbound complexes.

In the carbon nanotube binding assay, a stock solution of 0.5% multiwalled carbon nanotubes (<8 nm diameter, Cheap Tubes Inc.) with 0.7% tween-20 in PBS is diluted 10× with Millipore water. Larger CNT bundles are removed by centrifugation at 14 000 g for 30 min. Before making the flow cell, 150 uL of the nanotube containing supernatant is dried on the coverslip and then rinsed with Millipore water. The DNA−peptide (DNA-CGGHWSAWWIRSNQS) is loaded in the channel at a concentration of 0.1 ng/μL in PBS (Phosphate buffered saline, pH 7.4) and incubated for 1 h at RT. A 1 mg/mL casein in PBS solution is then incubated in the channel for 30 min. At the same time, 1.26 μm polystyrene beads coated with streptavidin (Spherotech) are also incubated in 1 mg/mL casein in PBS for 30 min. The beads are then loaded into the channel, incubated for 30 min, and a final wash is completed with 100 μL of the 1 g/L casein solution. Controls with only Tween-20 (no CNT) dried on the slip show 10× less beads attached on the surface.

In the antibody−fluorescein binding assay, mouse monoclonal antibody (clone 4−4−20, Invitrogen) is loaded in the channel at a concentration of 15 μg/μL in PBT (Phosphate buffer, with 0.1% Tween-20 pH 7.4) and incubated for 40 min. 1 mg/mL casein in PBT is then incubated in the channel for 20 min at RT. Avidin coated polystyrene microspheres (Spherotech) with diameters of 0.56 or 0.76 μm are also incubated in 1 mg/mL casein for 30 min at RT. Then the beads are loaded in the channel, incubated for 30 min at RT, and a final wash with 1 mg/mL casein solution in PBST is completed to remove unattached beads.

Concentrations of antibody, fluorescein-conjugated DNA, or peptide-conjugated DNA, are adjusted to maximize the number of single molecule tethers present and minimize rebinding events. Control scenarios using DNA tethers with only the terminal amine or the terminal amine attached to the sulfo-SMCC, but without a peptide demonstrate negligible interaction or attachment to the surface.

2.2. Optical Trap Based Force Spectroscopy. Experiments are performed using an optical trap as described previously.[17] Briefly, it consists of a 10 W, 1064 nm trapping laser (IPG Photonics) that is steered with acoustic optic deflectors (IntraAction) before being focused at the sample plane with a 100× 1.4 NA objective (Nikon). A second 975 nm laser beam (Avanex) is passed through the objective and is projected on a position-sensitive device providing nanometer scale position resolution. A piezo driven stage (Physik Instrumente) provides controllable motion.

Single molecule tethers are centered perpendicular to the optical axis by repeated tether stretching at very low force. Centering is crucial to provide a constant pulling rate along a single axis and collecting a consistent data set. The centering procedure also provides an estimate of the DNA tether length and symmetry allowing for quick detection of beads with multiple or incorrectly attached tethers. After centering, the trap stiffness is increased to approximately 0.25 pN/nm (0.3−0.5 pN/nm) for the peptide aptamer (fluorescein−antifluorescein) rupture and the tether is stretched by translating the sample relative to the trap with the piezo stage at a constant speed of 40 μm/s for the aptamer binding assays and 40, 80. or 120 μm/s for the antibody binding assay, until the bond ruptured. After rupture, each bead is run through an automated protocol to calibrate the exact position and forces applied. Trap stiffness is obtained using the equipartition method.[18] Each event is analyzed for rupture force, loading rate, and an approximate tether length. A representative rupture curve is shown in Figure 2.

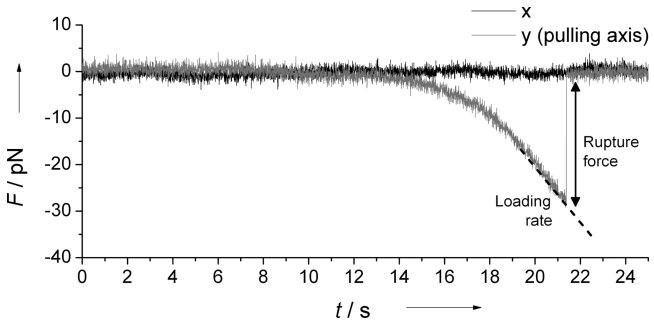

Figure 2. Representative force curve showing a rupture event. Rupture forces and loading rates, dashed line, are directly measured from rupture curves.

Events showing multiple, or stepped breaks, too short or too large tether lengths as well as those where the bead did not return to the center of the trap after the rupture are discarded.

2.3. Avoiding Carbon Nanotubes Heating. Carbon nanotubes (CNT) absorb in the near IR and may generate heat when illuminated by the trapping laser. To avoid this, while the beam center is within 0.5 μm of the peptide−CNT bond, an interposable filter that blocks 90% of the light intensity is placed in front of the laser beam. To test if this procedure prevents temperature increase in the vicinity of the peptide−MWNT interface, rupture forces are measured at two laser powers of 338 mW and 520 mW, measured before entering microscope objective. At low laser power, a mean rupture force of 25.5 pN is found with a mean loading rate of 5.7 pN/s. At high laser power, a comparable mean rupture force of 22.5 pN is found. The slight decrease can be attributable to a slower loading rate of 4.6 pN/s. Overlapping distributions suggest CNT heating is not occurring and the two data sets are combined into a single histogram.

2.4. Data Analysis. Rupture forces and loading rates are extracted directly from the bead position, obliviating the need for DNA tether stiffness correction.[19] Data analysis is performed using automated routines in MATLAB (MathWorks) and Igor Pro (Wavemetrics). A correction to the applied force based on the pulling angle is made by dividing the measured force by the cosine of the angle between the DNA linker and the surface, assuming that the bead is almost in contact with the surface. The pulling angle is 14.6° for the glass binding aptamer assay, 17.5° for the polystyrene, 20.3° for the CNT, and 25.3° for the fluorescein−antifluorescein unbinding assay with the 0.56 μm beads and 30.3° for the assay with 0.76 μm beads. The force applied to the adhesion is that which is directly applied to the bead as the DNA is assumed to be perfectly elastic and the DNA and peptide can be modeled as two spring in series.

3. RESULTS AND DISCUSSION

3.1. Peptide Aptamers Show Comparable Rupture Force. Peptide aptamers with affinity for glass,[14] polystyrene,[13] and carbon nanotubes[12] are studied. The glass-binding peptide (RSGRRRSHHHRL) is highly positively charged as two-thirds of its residues are either Arg or His, suggesting that binding to the negatively charged glass surface is electrostatically driven. The polystyrene-binding peptide (RAFIASRRIKRP) is similarly enriched in positive amino acids and interacts electrostatically with the surface of polystyrene microbeads that carry a slight negative charge from the sulfate ester. In contrast, the highly hydrophobic carbon nanotube (CNT)-binding peptide (HWSAWWIRSNQS)

Table 1. Rupture Forces and Loading Rates Measurements for Aptamer−Surface and Fluorescein−Antibody Unbinding

		rupture force[b]		loading rate[c]	
interaction	N^a	average	std dev	average	std dev
glass/aptamer	74	19.2	6.3	2.2	0.8
polystyrene/aptamer	72	29.0	7.5	7.3	2.5
CNTs/aptamer	102	24.2	9.5	5.2	3.1
fluorescein/antibody	157	30.4	21.5	6.1	5.1
fluorescein/antibody	62	41.3	25.2	11.8	8.6
fluorescein/antibody	79	59.8	30.2	24.7	13.3

[a] Number of single-molecule measurements. [b] Units are pN. [c] Units are pN·s^{-1}.

suggests hydrophobically driven interactions. Glass peptide adhesion is not limited to the surface it was selected for, as it has also been found to bind CdS, ZnS, and Au.[14] Since the polystyrene-binding mechanism is similar, nonspecific adhesion would be likely. However, due to the diversity in surface charge magnitude and spacing at the atomic scale for different surfaces, the avidity and strength of the adhesion would be expected to vary.

Conveniently, the glass- and polystyrene-binding aptamers attach directly to the glass coverslips and the polystyrene beads typically used in optical trapping assays, thus simplifying the setup by removing the need for additional surface functionalization. Carbon nanotube binding aptamers are studied by immobilizing CNTs on glass coverslips (Figure 1 and Table 1). As CNTs absorb in the NIR and generate heat when illuminated with the 1064 nm trapping laser, precautionary measures described above are taken to ensure that CNTs do not heat during the rupture event. Single molecule rupture force distributions, Figure 3, exhibit average rupture forces of 19 pN for glass binding aptamers, 29 pN for polystyrene, and 24 pN for CNTs with average loading rates of 2.2, 7.3, and 5.2 pN·s^{-1} respectively.

The specific conformation the peptide takes on the surface is currently unknown. This, in combination with the amorphous surface of glass and polystyrene, makes it difficult to determine if the interactions the peptide makes with the surface are broken simultaneously or sequentially. Thus, we anticipate that the unbinding distribution becomes broader as it reflects the overlap or masking of multiple individual distributions for each potential binding orientation and unbinding trajectory. A shorter distance to the transition state is obtained as the unbinding distribution becomes wider. However, for the polystyrene binding apatamer we are measuring only one unbinding trajectory, as the bead can freely rotate within the trap forcing a sequential unbinding of the adhesion.

3.2. Antifluorescein Rupture from Fluorescein Increases from 30 to 60 pN with Loading Rate. To validate our method and compare our results to a different biomolecular interaction, we studied the attachment of an antibody/antigen pair. The adhesion of the murine monoclonal antibody, clone 4−4−20, to the fluorescein antigen is probed. Here, rupture force histrograms are obtained at loading rates of 6.1, 11.8, and 24.7 pN·s^{-1}, Figure 4. Average rupture forces are found to increase with the loading rates from 30 to 60 pN.

3.3. Model Fitting Allows Extracting Kinetic and Energetic Parameters. Theoretical advances allow for extracting kinetic and energetic information from single molecule pulling experiments.

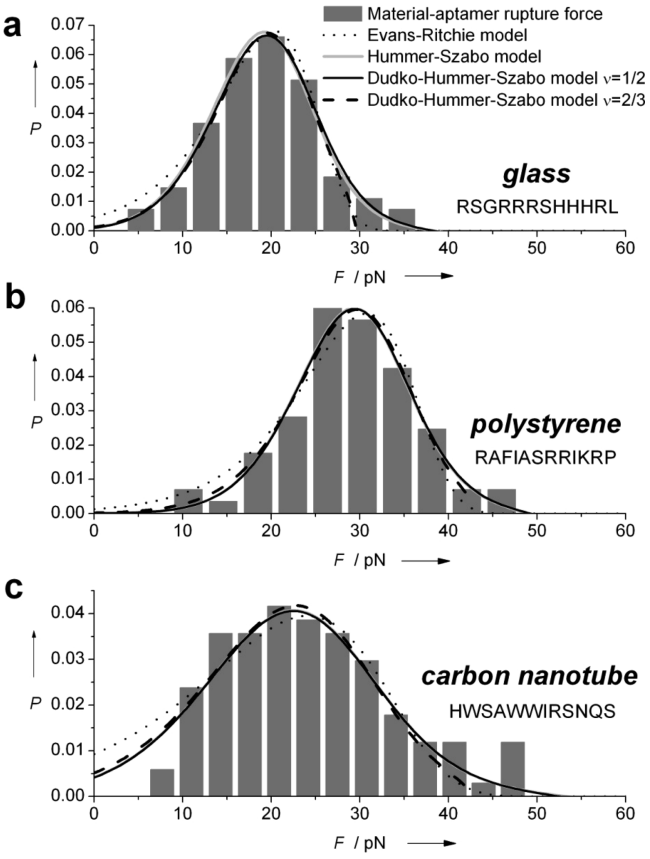

Figure 3. Rupture-force probability distributions for peptide aptamer binding to (a) glass, (b) polystyrene, and (c) carbon nanotubes. Histograms are fit to the model of Evans−Ritchie[21] (dotted line), Hummer−Szabo[22] (gray), and Dudko et al.[23] assuming a cusp-shaped (ν = 1/2, black solid line) or a linear-cubic (ν = 2/3, black dashed line) energy barrier.

Bell,[20] Evans, and Ritchie[21] described single molecule bond rupture as a thermally activated escape along a reaction coordinate, x, over a potential barrier, providing general shape of population distributions and exponential dependence of rupture time versus load. This "phenomenological" model assumes that the potential barrier is very tall and that the transition state remains stationary during pulling. Hummer and Szabo[22] have refined this model by considering the system as being pulled by a harmonic spring moving at constant velocity, with a harmonic underlying free-energy surface. More recently, Dudko, Hummer, and Szabo[23] also considered cusps and cubic-linear shaped transition state surfaces. A wide variety of pioneering theoretical[21−24] and experimental[25−29] work in this area can be found in literature. Models are still advancing to include probability of rebinding.[30] The antibody and aptamers rupture force histograms are fit here to the Evans−Ritchie model,[21] Hummer−Szabo model,[22] and Dudko−Hummer−Szabo model[23] assuming a cusp-shaped (ν = 1/2) or a linear-cubic (ν = 2/3) energy barrier, to provide estimates for τ_0, $x^{\ddagger}$, and $\Delta G^{\ddagger}$. The following equations for distribution of forces at rupture, $P(F)$, are used for the Evans−Ritchie model fitting:

$$P(F) = \frac{k_0}{\dot{F}} \exp\left\{\frac{Fx^{\ddagger}}{k_B T} - \frac{k_B T k_0}{\dot{F}x^{\ddagger}}\left(e^{Fx^{\ddagger}/k_B T} - 1\right)\right\}$$

for the Hummer-Szabo model:

$$P(F) = \dot{F}^{-1}[-\dot{S}(t^*)]_{t^* = (F + k_B T k_s x^{\ddagger})/\dot{F}}$$

with

$$S(t) = \exp\left[-\frac{k_B T k_0 e^{-k_s x^{\ddagger 2}/2}}{\dot{F} x^{\ddagger}} \left(\frac{k_m}{k_m + k_s} \right)^{3/2} \left(e^{\frac{\dot{F} x^{\ddagger} t}{k_B T}} - \left(\frac{\dot{F} t}{k_B T} \right)^2 / 2(k_m + k_s) - 1 \right) \right]$$

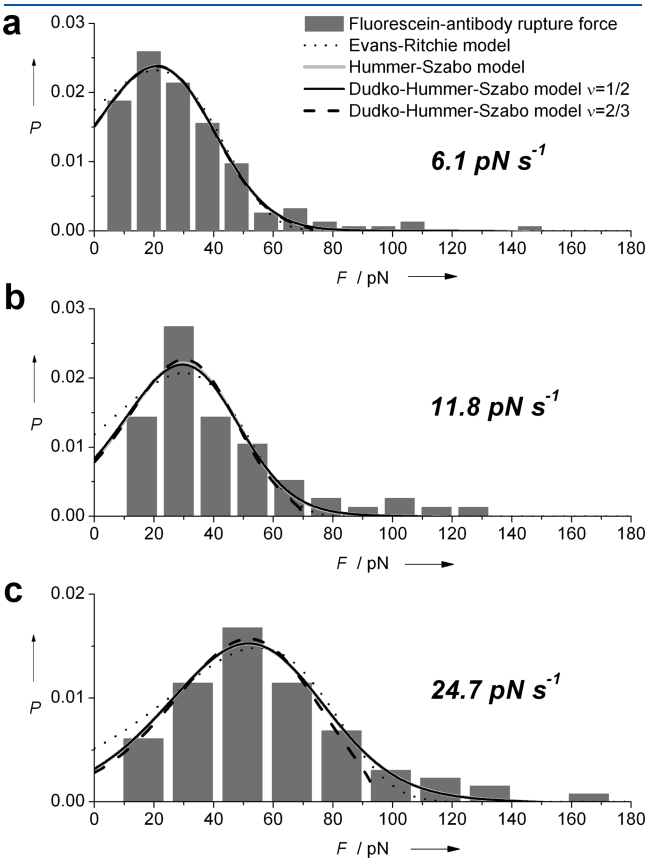

Figure 4. Rupture-force probability distributions for fluorescein binding to antibody 4−4−20 at average loading rates of (a) 6.1, (b) 11.8, and (c) 24.7 pN·s^{-1}. Histograms are fit to the model of Evans−Ritchie[21] (dotted line), Hummer−Szabo[22] (gray), and Dudko et al.[23] assuming a cusp-shaped (ν = 1/2, black solid line) or a linear-cubic (ν = 2/3, black dashed line) energy barrier.

and

$$k_m = \frac{2\Delta G^{\ddagger}}{k_B T x^{\ddagger 2}}$$

and for the Dudko−Hummer−Szabo model:

$$P(F) = \dot{F}^{-1} k(F) \exp\left[k_B T k_0 / x^{\ddagger} \dot{F} \right] \times \exp\left[-k_B T k(F) / x^{\ddagger} \dot{F} \left(1 - \frac{\nu F x^{\ddagger}}{\Delta G^{\ddagger}} \right)^{1 - 1/\nu} \right]$$

with

$$k(F) = k_0 \left(1 - \frac{\nu F x^{\ddagger}}{\Delta G^{\ddagger}} \right)^{1/\nu - 1} \times \exp\left\{ \frac{\Delta G^{\ddagger}}{k_B T} \left[1 - \left(1 - \frac{\nu F x^{\ddagger}}{\Delta G^{\ddagger}} \right)^{1/\nu} \right] \right\}$$

k_0 is the intrinsic off rate constant at zero force ($k_0 = \tau_0^{-1}$), k_B is Boltzmann's constant, T is the absolute temperature, $\dot{F}$ is the loading rate, k_s is the force constant of the pulling apparatus scaled by $k_B T$, and $S(t)$ is the survival probability of the system.

Tables 2 and 3 show the results from fitting our data with several of these models assuming either a cusp-shaped or a linear-cubic free energy profile.[31] Fits with either energy profiles lead to comparable estimates, however slightly smaller τ_0, $x^{\ddagger}$, and $\Delta G^{\ddagger}$ values are found for the linear-cubic profile in the cases of peptide aptamer adhesion.

Energy landscapes of peptide aptamers and antibody/fluorescein interactions are shown in Figures 5 with energy wells represented as harmonic potentials. The transition state distance $x^{\ddagger}$, along the pulling direction is extended for the glass and polystyrene binders (~1.6 nm) compared to that of the CNT binding peptides (0.8 nm). The lengths are consistent with the shorter range of hydrophobic interactions compared to electrostatic. In addition, comparisons of τ_0 and $\Delta G^{\ddagger}$ indicate that adhesion is the weakest for the CNT binding aptamers and the strongest for the polystyrene binding aptamers with $\Delta G^{\ddagger}$ varying from 5.2 $k_B T$ for CNT, up to 10.5 $k_B T$ for polystyrene assuming a cusp shaped barrier. Values for τ_0 follow the same trend with 46 s for CNT, 423 s for glass, and 2945 s for polystyrene.

For the antibody-fluorescein interaction, fitted parameters for the three loading rates are in close agreement and have a relative standard deviation of only ~10%, highlighting the remarkable consistency of our method. Furthermore, Boder et al.[32] measured a bulk τ_0 value of 39.8 s for clone 4−4−20,

Table 2. Kinetic and Energetic Parameters for Aptamer-Surface Unbinding, from Fits to the Model of Evans-Ritchie,[21] Hummer-Szabo,[22] and Dudko et al.[23] Assuming a Cusp-Shaped (ν = 1/2) or a Linear-Cubic (ν = 2/3) Energy Barrier

						Dudko−Hummer−Szabo model					
	Evans−Ritchie model		Hummer−Szabo model			ν = 1/2			ν = 2/3		
interaction	τ_0[a]	$x^{\ddagger}$[b]	τ_0	$x^{\ddagger}$	$\Delta G^{\ddagger}$[c]	τ_0	$x^{\ddagger}$	$\Delta G^{\ddagger}$	τ_0	$x^{\ddagger}$	$\Delta G^{\ddagger}$
glass/aptamer	96.9	0.747	457.1	1.586	7.47	422.9	1.568	7.38	333.5	1.340	6.48
polystyrene/aptamer	109.5	0.652	3366.7	1.763	10.60	2945.2	1.732	10.48	725.1	1.218	8.61
CNTs/aptamer	20.7	0.404	46.4	0.807	5.28	46.4	0.813	5.24	37.4	0.678	4.71

[a] Units are s. [b] Units are nm. [c] $\Delta G^{\ddagger}$ is in $k_B T$ units.

dx.doi.org/10.1021/jp1031493 |J. Phys. Chem. A 2011, 115, 3657–3664

Table 3. Kinetic and Energetic Parameters for Antifluorescein 4−4−20 Unbinding from Fluorescein, from Fits to the Model of Evans−Ritchie,[21] Hummer−Szabo,[22] and Dudko et al.[23] Assuming a Cusp-Shaped ($\nu = 1/2$) or a Linear-Cubic ($\nu = 2/3$) Energy Barrier

						Dudko−Hummer−Szabo model					
	Evans−Ritchie model		Hummer−Szabo model			$\nu = 1/2$			$\nu = 2/3$		
loading rate	τ_0[a]	$x^\ddagger$[b]	τ_0	$x^\ddagger$	$\Delta G^\ddagger$[c]	τ_0	$x^\ddagger$	$\Delta G^\ddagger$	τ_0	$x^\ddagger$	$\Delta G^\ddagger$
6.1 pN·s^{-1}	9.34	0.171	10.9	0.263	3.65	10.8	0.262	3.63	10.8	0.248	2.99
11.8 pN·s^{-1}	7.13	0.176	10.5	0.318	4.14	10.1	0.311	4.09	10.8	0.308	3.54
24.7 pN·s^{-1}	7.84	0.144	12.8	0.259	4.65	12.7	0.257	4.66	14.4	0.260	4.01

[a] Units are s. [b] Units are nm. [c] $\Delta G^\ddagger$ is in k_BT units.

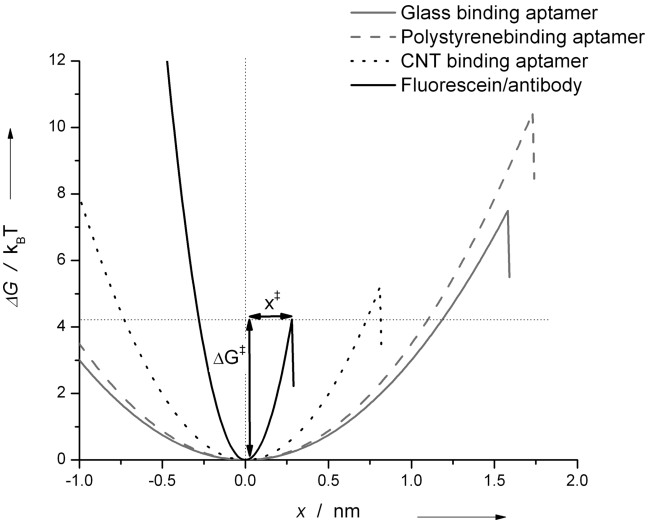

Figure 5. Energy landscape from parameters fitted using the model of Dudko et al.[23] assuming a cusp shaped ($\nu = 1/2$) barrier, with energy wells represented as harmonic potentials.

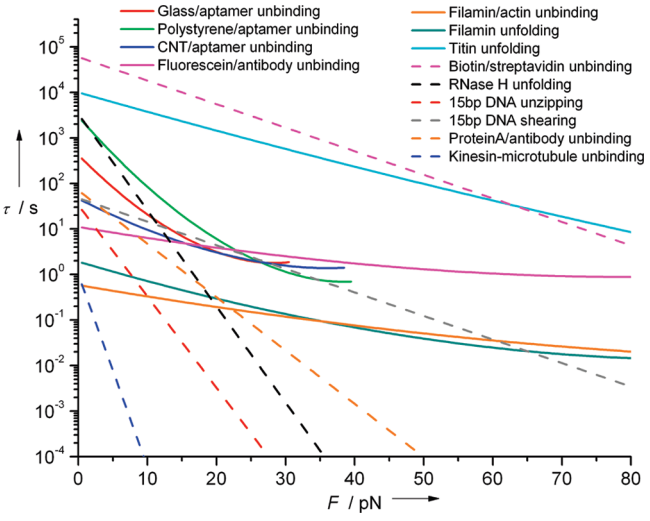

Figure 6. Lifetime $\tau(F)$ as a function of the applied force (F) compared to curves derived from parameters obtained from literature (Table 4) for a range of biological interactions. Kinesin−microtubule interaction is for single headed kinesin in ADP state with plus-end loading. $\tau(F)$ is obtained assuming a cusp-like barrier[23] when $\Delta G^\ddagger$ available, solid lines; otherwise, Evans−Ritchie model[21] is used with $\nu = 1$, dashed lines.

which is compatible with our results when considering differences in buffer conditions.

$\Delta G^\ddagger$ for antibody−fluorescein unbinding is 4 k_BT, which is lower than that of aptamers (5−10 k_BT). Transition state distance, $x^\ddagger$, is nearly an order of magnitude longer for peptide adhesion than antibody binding. The larger $x^\ddagger$ and $\Delta G^\ddagger$ obtained for peptide aptamers are rationalized by considering the solvent accessible surface area, which gives an estimate for the number of noncovalent interactions involved in the bond. Fluorescein has a solvent accessible surface area of 5 nm^2, calculated by using VMD.[33] Accessible surface area of peptides are computed by summing the surface areas of each amino acid side chain,[34] assuming that they adopt an extended conformation. Using this method, a similar surface area of 17 nm^2 is obtained for each aptamer in extended conformation, three times more than that of the antibody. Aptamer−materials interactions could therefore involve a higher number of electrostatic, hydrogen-bonding and van der Waals forces, which is evidenced by larger $x^\ddagger$ and $\Delta G^\ddagger$. Lifetime under no load is lower (11 s) for antifluorescein. However, under high forces the antibody lifetime surpasses that of aptamers.

It is important to note that our rupture experiments are done in the low loading rate regime (2−25 pN·s^{-1}). Alternate kinetic and energetic parameters might have been found in a higher loading rate regime.[35,36] However, extrapolated unloaded off-rates (or lifetimes) are most valid when extracted from lower loading rate force measurements, which approach unloaded conditions.

3.4. Comparison of Lifetime-Force Relationships with Other Bimolecular Interactions. Lifetime-force relationships of peptide aptamers and antibody/fluorescein interactions are obtained from the following equation:[31]

$$\tau(F) = \tau_0\left(1 - \frac{\nu F x^\ddagger}{\Delta G^\ddagger}\right)^{1-1/\nu} \times \exp\left[-\Delta G^\ddagger/k_BT\left[1 - \left(1 - \frac{\nu F x^\ddagger}{\Delta G^\ddagger}\right)^{1/\nu}\right]\right]$$

where ν depends on the energy profile (1/2 for cusp shaped, 2/3 for linear-cubic, and 1 for the phenomenological model). Figure 6 shows the aptamer and antibody lifetimes compared to several other biomolecular interactions that have been studied with single molecule force spectroscopy. Parameters for these interactions are shown in Table 4. Unloaded off rates (τ_0^{-1}) span

Table 4. Parameters (τ_0, $x^{\ddagger}$, $\Delta G^{\ddagger}$ and ν) for Interactions Shown in Figure 6, and Loading Rates at Which Those Interactions Were Probed

interaction	τ_0 (s)	$x^{\ddagger}$ (nm)	$\Delta G^{\ddagger}$ (k_BT)	ν	loading rate (pN·s^{-1})	refs
filamin/actin unbinding	0.59	0.27	5.6	1/2	400−2000	37
filamin unfolding	1.92	0.46	6.8	1/2	400−2000	37
titin unfolding	10^4	0.42	19.5	1/2	6000	22, 38
biotin/streptavidin unbinding	5.99×10^4	0.49		1	100−1000	39
RNaseH unfolding	3.33×10^3	2.0		1	13−53	40
15bp DNA unzipping	33.3	1.9		1	11	16
15bp DNA shearing	47.6	0.49		1	24	16
protein A/antibody undinbing	69.9	1.1		1	0.3−500	41
kinesin−microtubule unbinding	1	4.0		1	5	42

several orders of magnitude. Slopes of τ(F) allow for comparison of relative barrier width $x^{\ddagger}$, with the longest $x^{\ddagger}$ for kinesin-microtubule unbinding and the smallest $x^{\ddagger}$ for antibody-fluorescein unbinding. A τ(F) plot also allows for comparison of spontaneous rupture ($\tau < 1$s). The fastest unbinding is observed for the molecular motor kinesin, which must readily break adhesions in order to produce processive motility. Nature tunes interactions balancing stability needed to make lasting bonds with requirements to break them within larger systems, which may require rearrangement or conformational change. For example, unbinding and unfolding of filamin require similar forces with a slight bias for filamin rupture at low loads and unfolding at higher.[37] Described more graphically, one can control interactions not only by identifying the intercept, or unloaded off rate, but by the slope of the curve.

4. CONCLUSIONS

In summary, optical tweezers are used for single molecule force spectroscopy studies of peptide adhesion to materials and antibody−fluorescein interaction. Energy landscapes are reconstructed using theoretical models. Free energies of bond rupture are all in the same order of magnitude with ∼5−10 k_BT for peptide aptamers and ∼3−5 k_BT for antifluorescein. We find that peptide aptamers are strong no load binders, yet at higher loads antifluorescein adheres better. The developed assay has great potential to assess new linkers for biomimetic self-assembly and to explore how their adhesion strengths compare to inter- and intramolecular interactions found in nature.

AUTHOR INFORMATION

Corresponding Author

*E-mail: matt.lang@vanderbilt.edu.

Present Addresses

[#]MRC Laboratory of Molecular Biology, Cambridge CB2 0QH, U.K.

[@]Chemical and Biomolecular Engineering, Vanderbilt University.

Author Contributions

[†]These authors contributed equally to this work.

ACKNOWLEDGMENT

We thank Singapore-MIT Alliance for Research and Technology (SMART), NSF Career Award 0643745, and NIH R21CA133576 for funding. We are thankful to Olga K. Dudko and Eric Krauland for helpful discussion.

REFERENCES

(1) Mayer, G. *Angew. Chem., Int. Ed.* **2009**, *48*, 2672.
(2) Ho, D.; Falter, K.; Severin, P.; Gaub, H. E. *Anal. Chem.* **2009**, *81*, 3159.
(3) Shao, N.; Wickstrom, E.; Panchapakesan, B. *Nanotechnology* **2008**, *19*, 465101.
(4) Wu, Y.; Sefah, K.; Liu, H.; Wang, R.; Tan, W. *Proc. Natl. Acad. Sci. U. S. A.* **2010**, *109*, 5.
(5) Li, Z.; Huang, P.; He, R.; Lin, J.; Yang, S.; Zhang, X.; Ren, Q.; Cui, D. *Mater. Lett.* **2010**, *64*, 375.
(6) Sullenger, B. A.; Gilboa, E. *Nature* **2002**, *418*, 252.
(7) Ng, E. W.; Shima, D. T.; Calias, P.; Cunningham, E. T.; Guyer, D. R.; Adamis, A. P. *Nat. Rev. Drug Discovery* **2006**, *5*, 123.
(8) Woodside, M. T.; Anthony, P. C.; Behnke-Parks, W. M.; Larizadeh, K.; Herschlag, D.; Block, S. M. *Science* **2006**, *314*, 1001.
(9) Hayashi, T.; Sano, K. I.; Shiba, K.; Kumashiro, Y.; Iwahori, K.; Yamashita, I.; Hara, M. *Nano Lett.* **2006**, *6*, 515.
(10) Lee, H.; Scherer, N. F.; Messersmith, P. B. *Proc. Natl. Acad. Sci. U. S. A.* **2006**, *103*, 12999.
(11) Sanghvi, A. B.; Miller, K. P.-H.; Belcher, A. M.; Schmidt, C. E. *Nat. Mater.* **2005**, *4*, 496.
(12) Wang, S.; Humphreys, E. S.; Chung, S. Y.; Delduco, D. F.; Lustig, S. R.; Wang, H.; Parker, K. N.; Rizzo, N. W.; Subramoney, S.; Chiang, Y. M.; Jagota, A. *Nat. Mater.* **2003**, *2*, 196.
(13) Kumada, Y.; Tokunaga, Y.; Imanaka, H.; Imamura, K.; Sakiyama, T.; Katoh, S.; Nakanishi, K. *Biotechnol. Prog.* **2006**, *22*, 401.
(14) Krauland, E. M. Towards Rational Design of Peptides for Selective Interaction with Inorganic Materials. Ph.D. Thesis, Massachusetts Institute of Technology: 2007.
(15) Svoboda, K.; Schmidt, C. F.; Schnapp, B. J.; Block, S. M. *Nature* **1993**, *365*, 721.
(16) Lang, M. J.; Fordyce, P. M.; Engh, A. M.; Neuman, K. C.; Block, S. M. *Nat. Methods* **2004**, *1*, 133.
(17) Brau, R. R.; Tarsa, P. B.; Ferrer, J. M.; Lee, P.; Lang, M. J. *Biophys. J.* **2006**, *91*, 1069.
(18) Lang, M. J.; Asbury, C. L.; Shaevitz, J. W.; Block, S. M. *Biophys. J.* **2002**, *83*, 491.
(19) Ray, C.; Brown, J. R.; Akhremitchev, B. B. *J. Phys. Chem. B* **2007**, *111*, 1963.
(20) Bell, G. I. *Science* **1978**, *200*, 618.
(21) Evans, E.; Ritchie, K. *Biophys. J.* **1997**, *72*, 1541.
(22) Hummer, G.; Szabo, A. *Biophys. J.* **2003**, *85*, 5.
(23) Dudko, O. K.; Hummer, G.; Szabo, A. *Phys. Rev. Lett.* **2006**, *96*, 108101.
(24) Zimanyia, E. N.; Silbey, R. J. *J. Chem. Phys.* **2009**, *130*, 171102.
(25) Rief, M.; Gautel, M.; Oesterhelt, F.; Fernandez, J. M.; Gaub, H. E. *Science* **1997**, *276*, 1109.
(26) Chang, K.-C.; Tees, D. F. J.; Hammer, D. A. *Proc. Natl. Acad. Sci. U. S. A.* **2000**, *97*, 11262.
(27) Fritz, J.; Katopodis, A. G.; Kolbinger, F.; Anselmetti, D. *Proc. Natl. Acad. Sci. U. S. A.* **1998**, *95*, 12283.

(28) Heinrich, V.; Wong, W. P.; Halvorsen, K.; Evans, E. *Langmuir* **2008**, *24*, 1194.
(29) van der Horst, A.; Forde, N. R. *Opt. Express* **2008**, *16*, 20987.
(30) Friddle, R. W. *Phys. Rev. Lett.* **2008**, *100*, 138302.
(31) Dudko, O. K.; Hummer, G.; Szabo, A. *Proc. Natl. Acad. Sci. U. S. A.* **2008**, *105*, 15755.
(32) Boder, E. T.; Midelfort, K. S.; Wittrup, K. D. *Proc. Natl. Acad. Sci. U. S. A.* **2000**, *97*, 10701.
(33) Humphrey, W.; Dalke, A.; Schulten, K. *J. Mol. Graph.* **1996**, *14*, 33.
(34) Miller, S.; Janin, J.; Lesk, A. M.; Chothia, C. *J. Mol. Biol.* **1987**, *196*, 641.
(35) Merkel, R.; Nassoy, P.; Leung, A.; Ritchie, K.; Evans, E. *Nature* **1999**, *397*, 50.
(36) Neuert, G.; Albrecht, C.; Pamir, E.; Gaub, H. *FEBS Lett.* **2006**, *580*, 505.
(37) Lee, H.; Pelz, B.; Ferrer, J. M.; Kim, T.; Lang, M. J.; Kamm, R. D. *Cell. Mol. Bioeng.* **2009**, *2*, 28.
(38) Carrion-Vazquez, M.; Oberhauser, A. F.; Fowler, S. B.; Marszalek, P. E.; Broedel, S. E.; Clarke, J.; Fernandez, J. M. *Proc. Natl. Acad. Sci. U. S. A.* **1999**, *96*, 3694.
(39) Yuan, C.; Chen, A.; Kolb, P.; Moy, V. T. *Biochemistry* **2000**, *39*, 10219.
(40) Cecconi, C.; Shank, E. A.; Bustamante, C.; Marqusee, S. *Science* **2005**, *23*, 2057.
(41) Salomo, M.; Keyser, U. F.; Struhalla, M.; Kremer, F. *Eur. Biophys. J.* **2008**, *37*, 927.
(42) Uemura, S.; Kawaguchi, K.; Yajima, J.; Edamatsu, M.; Toyoshima, Y. Y.; Ishiwata, S. *Proc. Natl. Acad. Sci. U. S. A.* **2002**, *99*, 5977.